Neutron diffraction studies of $Nd_{1-x}Pr_xBa_2Cu_3O_{7-\delta}$: Evidence for hole localization

S. R. Ghorbani,[1,2] M. Andersson,[1] and Ö. Rapp[1]
[1]*Solid State Physics, Department of Microelectronics and Information Technology, KTH Electrum 229, SE-164 40 Kista, Sweden*
[2]*Department of Physics, Sabzevar Teacher Training University, P.O. Box 397, Sabzevar, Iran*
(Received 20 November 2001; revised manuscript received 26 September 2003; published 13 January 2004)

Sintered samples of $Nd_{1-x}Pr_xBa_2Cu_3O_{7-\delta}$ with $x=0$, 0.05, 0.10, 0.15, 0.20, and 0.30 have been studied by neutron diffraction, x-ray diffraction, and resistivity measurements. Sample stoichiometry was carefully checked. Atomic distances within the unit cell and the oxygen content were shown to be almost independent of Pr doping. Bond valence sums (BVSs) were calculated from the neutron diffraction data assuming either a constant valence or a mixed valence for Cu and Pr ions. The planar Cu2 valence is independent of Pr doping and the chain Cu1 valence is roughly constant, while the hole concentration in the planes and chains decrease with increasing Pr doping for both BVS calculation methods. All together, this indicates that hole localization on the Nd(Pr) site is a main reason for the decrease of the hole concentration in the planes. A consistent relation between the hole concentration in the planes calculated from the constant valence method and the depression of the critical temperature is also obtained, both for Pr-doped Nd-123 and for Y(Pr)-123 studied previously.

DOI: 10.1103/PhysRevB.69.014503 PACS number(s): 74.72.Jt, 74.25.Fy, 74.62.Dh

I. INTRODUCTION

It is well known that replacing yttrium in $YBa_2Cu_3O_{7-\delta}$ (Y-123) by different rare earth elements usually does not affect superconductivity except for Pr. However, substitution of Pr for R in $RBa_2Cu_3O_7$, (R=rare earth) leads to a rapid decrease of the superconducting transition temperature, T_c, and superconductivity is lost for substitution levels, x, larger than a critical level, x_c, which depends on the R ion. $x_c \approx 0.67$ and 0.32 was observed for Pr-doped Y- and Nd-123, respectively.[1] Different qualitative models[2–5] have been proposed to describe the suppression of superconductivity by Pr, like hole filling, hole localization, hybridization of Pr with the electrons in the CuO_2 plane, and magnetic pair breaking due to the Pr magnetic moment. The recent observation of superconductivity in samples of $PrBa_2Cu_3O_7$ synthesized by pulsed laser deposition or by the floating-zone method[6,7] further complicates the understanding of the role played by Pr in the suppression of T_c. Inhomogeneous sample properties found in these samples, and the possibility of Ba on Pr site,[6–8] raises the question how details of the stoichiometry may affect sample properties also for dilute solutions of Pr in 123 samples.

The high-T_c cuprate superconductors appear to have a common, approximately parabolic dependence of T_c upon hole concentration in the planes, p. T_c rises from zero at about $p_{\min}\approx 0.05$ to a maximum, $T_{c,\max}$ at $p\approx 0.16$ and then falls to zero at about $p_{\max}\approx 0.27$.[9] Another useful approach to empirically describe T_c in high-T_c superconductors was found by Neumeier *et al.* in $Y_{1-x-y}Pr_xCa_yBa_2Cu_3O_{7-\delta}$.[3] They suggested that T_c could be described by a parabolic hole doping term and a linear term originally assumed to be due to magnetic pair breaking:

$$T_c(x,y)=T_c(0)-A(\alpha-\beta x+y)^2-Bx,$$

$$0\leqslant x\leqslant 0.2 \quad \text{and} \quad 0\leqslant y\leqslant 0.2. \qquad (1)$$

Here $T_c(0)$ is the maximum possible value of T_c, y and x represent hole generation by Ca ions and hole filling by Pr, respectively. α is the optimal hole concentration and β is the fraction of a hole filled by each Pr ion. In Eq. (1), β is the deviation of the valence of Pr from +3. Later alternative mechanisms have been advanced.[5] However, Eq. (1) remains a useful empirical summary of the change of T_c with doping concentration in different 123 superconductors, and has been used frequently.

With Pr as a doping element of concentration limited to the dilute region of Eq. (1), it is found that β is close to 1,[3,10–13] indicating that Pr has a valence close to +4 and causes hole filling or localization. Doping with equal amounts of Pr and Ca on rare earth site is illustrative. The parabolic term in Eq. (1), representing charge variation, is then suppressed, and T_c is linear in doping concentration.[11–13] This is in similarity with the corresponding doping of Th^{4+}-Ca^{2+} in Nd-123,[14] and indicates that a characteristic impurity effect can be isolated by charge neutral dopings. Other results suggesting a larger Pr valence at low concentrations include the observation that features in the x-ray absorption spectra of Y(Pr)-123 ascribed to Pr^{4+} displayed a decreasing intensity with increasing Pr concentration,[15] and the finding that the variation of the average CuO_2 plane distance with an average ionic radius at low Pr doping concentrations in Y-(Ref. 16) and Nd-based[12] samples could be better described with Pr^{4+} than with Pr^{3+} ions.

A clue to reconciliation between these observations and abundant results in the literature of a Pr^{3+} state comes from the observation that most of these latter reports have studied samples with Pr concentration $x\geqslant 0.2$. In fact, several results suggest a valence shift at about this concentration. That is, in Nd(Pr)-123 the strong initial depression of the Hall number with doping was found to flatten out and to become roughly constant above about $x\approx 0.15$.[17] In alloy systems where there are marked changes in bond lengths with doping, characteristic changes in structural parameters can be observed, such as in $Gd_{1-x}Pr_xBa_2Cu_3O_{7-\delta}$ where the c-axis length first de-

creased up to about $x \approx 0.2$, and then increased slowly for larger x,[18] in qualitative agreement with the variation of ionic radii in the sequence $Pr^{4+} < Gd^{3+} < Pr^{3+}$. The resistivity studies by Tomkowicz[19] suggested a change of Pr valence from 4^+ to 3^+ at about $x = 0.2$ in $Ho_{1-x}Pr_xBa_2Cu_3O_{7-\delta}$.

A third approach to understanding the role of doping and changes of T_c is calculations of bond valence sums (BVSs). In this method the valence of an atom is taken to be distributed between its bonds as further described below. This approach has been widely used for high-T_c superconductors, e.g., in studies of T_c as a function of hole density in the planes $V_{\text{-pl}}$, calculated from BVS valences for the planar atoms.[20] A striking example is the closely similar relation $T_c = T_c(p)$ obtained with the hole density from BVSs or from other methods, showing that BVS calculations in 123 compounds can be quantitatively precise.[21] It should be noted however, that the BVS method is a semiempirical method. Its main advantage is therefore as a sensitive tool to give trends rather than absolute values for changing valences in a set of related alloys.

Neutron diffraction is useful in order to understand the role of Pr doping on structural and superconducting properties of *R*-123 systems. Previous studies in Pr-doped 123 compounds can be briefly summarized as follows. In Y(Pr)-123, Neumeier *et al.*[22] found that the distance between the planar Cu and apex oxygen positions increased with increasing Pr concentration and also that the distance between oxygen atoms in nearby planes in general increased. Kramer *et al.*[23] showed that a substantial fraction of the Pr ions entered the Nd sites in $Nd_{1.05}Ba_{1.95-x}Pr_xCu_3O_{7-\delta}$. The results for the doping dependence of the CuO_2 plane distance in Ca-Pr-doped Nd- and Y-123, quoted above,[12,16] were also based on neutron diffraction.

The aim of the present paper is to further clarify the role of Pr in a 123 host. As noted from the Hall effect in Nd(Pr)-123 and from the *c*-axis lattice parameter of Gd(Pr)-123,[17,18] a charge filling picture is incomplete. The strong values of *B* of Eq. (1) found for Pr-doped 123 samples also show that $T_c(x)$ cannot be explained only by charge filling. What is the nature of the additional depression of T_c? We have studied this question by neutron diffraction of $Nd_{1-x}Pr_xBa_2Cu_3O_{7-\delta}$. Sample preparation and characterization, and the measurement techniques are described in Sec. II, and details of the BVS calculations are given in Sec. III. In Sec. IV the results and analyses from resistivity measurements, neutron diffraction, and BVS calculations are described. In Sec. V the main results are discussed and briefly summarized. It is found that in addition to the hole filling at low Pr concentration, T_c is depressed due to a continuous decrease of $V_{\text{-pl}}$. The structural result suggest that holes localize on the Nd(Pr) site. The similarity of these results and calculations for the structurally different Y(Pr)-123 system, with general results for $p_{\min}$ at $T_c = 0$ suggest that hole localization is a common mechansm for depression of T_c in Pr-doped *R*-123.

II. SAMPLE CHARACTERIZATION AND EXPERIMENTAL TECHNIQUES

Samples of $Nd_{1-x}Pr_xBa_2Cu_3O_{7-\delta}$, with $x = 0$, 0.05, 0.10, 0.15, 0.20, and 0.30, were prepared by standard solid-state methods. Starting materials were high purity Nd_2O_3, $BaCO_3$, CuO, and Pr_6O_{11}. The samples were pressed into pellets and calcinated at 900, 920, and 920 °C in air with intermediate grindings. They were then annealed in flowing oxygen at 460 °C for three days and the temperature was finally decreased to room temperature at a rate of 12 °C/h.

The samples were characterized by x-ray powder diffraction (XRD). The XRD patterns were recorded in a Guinier-Hägg focusing camera using Cu$K\alpha$ radiation with Si as an internal standard, and the photographs were evaluated in a microdensitometer system.[24] This is a sensitive technique for detection of impurity phases with an estimated sensitivity level of a few percent of crystalline impurities. The XRD results for Pr-doped Nd-123 samples displayed a single-phase orthorhombic structure at all doping levels.

The electrical resistivity was measured with a standard dc four-probe method. Electrical leads were attached to the samples by silver paint and heat treated at 300 °C in flowing oxygen for half an hour, which gave contact resistances of order 1–2 Ω.

Neutron diffraction measurements were performed at the Swedish research reactor *R*2 in Studsvik. This instrument is equipped with a double monochromator consisting of the (220) surfaces of two copper crystals, which gave a wavelength 1.470 Å. The neutron flux at the sample position was about 2×10^6 cm^{-2} s^{-1}. The powdered samples were placed in 6 mm diameter vanadium tubes, and data were collected with 35 ^{3}He detectors which scanned a 2θ range of 4.00°–132.92° in steps of 0.08°.[25] Structure refinements were performed with the Rietveld method[26] using the FullProf software and the orthorhombic space group *Pmmm*. Refinements were performed both with anisotropic and isotropic displacement parameters at the chain oxygen sites, while isotropic parameters were used at all other atomic sites. For structure refinement most atomic positions were considered to be fully occupied, with the exception of the chain oxygen O1, and the O5 position along the *a*-axis direction, in order to register any oxygen disorder and to determine the oxygen concentration.

Particular attention has been paid to the atomic occupancy on the Nd and Ba sites. The samples with $x = 0$ and 0.30 were examined in a scanning electron microscope equipped with an energy dispersive spectrometer (EDS). No impurities were observed. The analyses indicated a constant ratio between the Ba and Cu contents on the different spots investigated and consistent results between the two samples studied. There is no evidence from EDS for Pr and Nd on a Ba site. However, it should be mentioned that in the analyses of the $x = 0.30$ sample, the relative Nd and Pr content slightly varied although their sum was constant.

In the Rietveld refinements, the Nd and Pr occupation factors on the Nd site, $n_{\text{Nd}}(\text{Nd})$ and $n_{\text{Pr}}(\text{Nd})$, were refined with the condition that there was no vacancy on the Nd site, i.e., $n_{\text{Nd}}(\text{Nd}) + n_{\text{Pr}}(\text{Nd}) = 1$. The possibility of Pr occupancy on the Ba site was also investigated,[27] as well as the Nd occupancy on the Ba site in a similar scheme, for the $x = 0$ sample.

For easy reference to structural notations a unit cell is shown in Fig. 1. Figures 2(a) and 2(b) show typical neutron

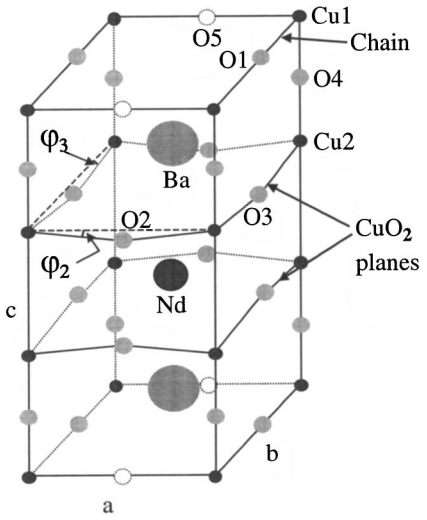

FIG. 1. The crystal structure and atomic notations of $NdBa_2Cu_3O_{7-\delta}$. Buckling angles are defined by φ_2 and φ_3.

diffraction results of $Nd_{1-x}Pr_xBa_2Cu_3O_{7-\delta}$ for $x=0$ and 0.30, respectively, displaying single-phase compounds.[28]

III. BOND VALENCE SUM (BVS) CALCULATIONS

The bond-valence sums of atom i is calculated from the empirically found relation between the bond strength and bond length,

$$V_i=\sum_j s_j=\sum_j \exp[(L_0-L_{ij})/0.37], \tag{2}$$

where s_j is the valence of an individual bond, and the sum is over all neighbors j.[29] L_0 is the length of a bond of a unit valence, and L_{ij} is the actual bond length between atoms i and j. L_0 was taken to be 1.600, 1.679, 1.70, and 2.154 Å for Cu^{1+}, Cu^{2+}, Cu^{3+},[20,30] and Pr^{4+},[12] respectively. For the other atoms L_0 was taken from Ref. 31.

It was pointed out that the copper bond valence sum V_{Cu2} and the oxygen bond-valence sums (V_{O2} and V_{O3}) are not independent variables,[20] and one should consider

$$\begin{aligned} V_+&=6-V_{Cu2}-V_{O2}-V_{O3},\\ V_{\text{-pl}}&=2+V_{Cu2}-V_{O2}-V_{O3}, \end{aligned} \tag{3}$$

where V_+ is the preference for distribution of holes on oxygen sites relative to copper sites, and $V_{\text{-pl}}$ is the hole density in the CuO_2 planes.

The hole density in the chains, $V_{\text{-ch}}$ was also calculated according to

$$V_{\text{-ch}}=V_{Cu1}-V_{O1}\times n_{O1}-V_{O5}\times n_{O5}. \tag{4}$$

n_{O1} and n_{O5} are the occupancy numbers of the two possible oxygen sites in the chain layer.

Two methods were used in the oxygen BVS calculations. The first one is a constant valence (CV) method.[20] In this method, Tallon[20] and Cava *et al.*[32] used only Cu^{2+} and Pr^{3+} in calculating the oxygen BVS. The second method takes

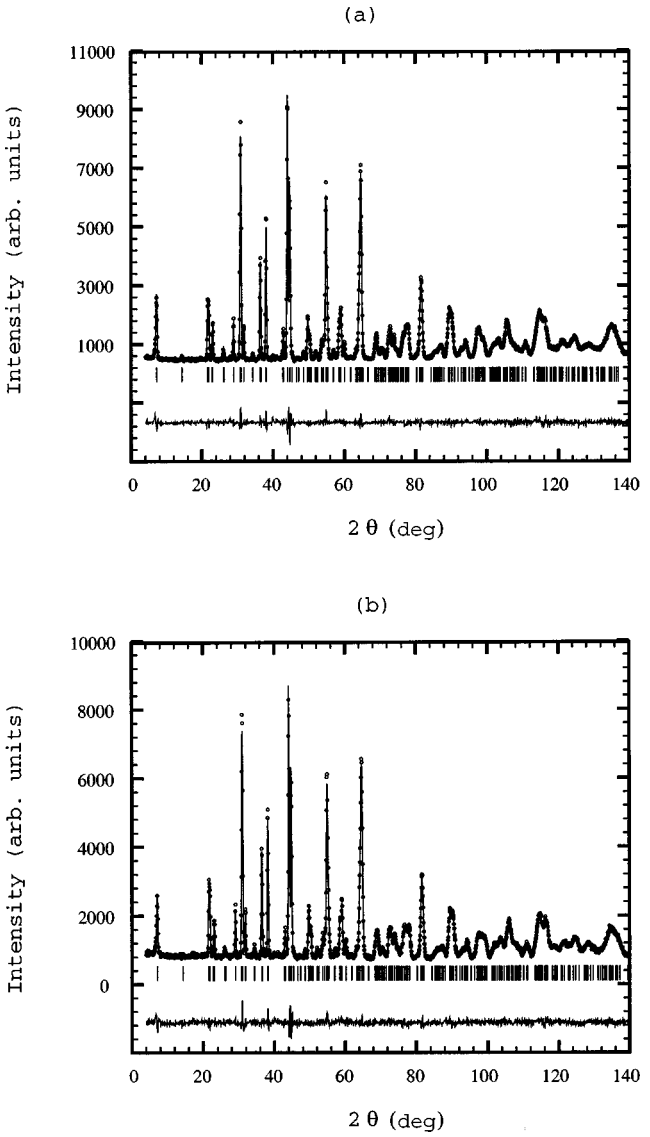

FIG. 2. Neutron diffraction results for $Nd_{1-x}Pr_xBa_2Cu_3O_{7-\delta}$ with (a) $x=0.0$ and (b) $x=0.30$. The position of the indexed lines and the differences between observed and calculated intensities are shown below the main panels.

mixed valences (MVs) into account.[12,33] The BVS for oxygen was calculated by allowing Cu^{1+}, Cu^{2+}, Cu^{3+}, Pr^{3+}, and Pr^{4+} valences. This gave somewhat higher valences than for the CV method. In the MV method, s_j in Eq. (2) for the Cu—O bond was obtained by $s(Cu)=s(Cu^{+3})r+s(Cu^{+2})\times(1-r)$ with $r=V_{Cu}-2$ for $V_{Cu}>2$, and for $V_{Cu}<2$: $s(Cu)=s(Cu^{+2})r+s(Cu^{+1})(1-r)$ with $r=V_{Cu}-1$. Further, $s(Pr)=s(Pr^{+4})r+s(Pr^{+3})(1-r)$ with $r=V_{Pr}-3$ for Pr—O. The bond valence between oxygen and rare earth position in, e.g., Nd(Pr)-123 is then $s(R)=s(Nd)\times n_{Nd}+s(Pr)\times n_{Pr}$, where n_{Nd} and n_{Pr} are the occupancies of Nd and Pr at the rare earth position, respectively. With respect to the clear results that Pr is 4 valent at low doping concentrations with an apparent shift to +3 above $x\cong 0.15$ we give preference to the CV method. However, both methods were used as a check on the BVS calculations.

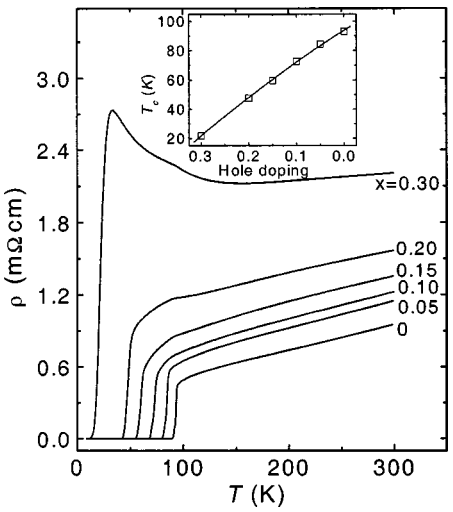

FIG. 3. The electrical resistivity ρ vs temperature T for $Nd_{1-x}Pr_xBa_2Cu_3O_{7-\delta}$ with $0 \leqslant x \leqslant 0.30$. Inset: The measured T_c vs hole doping for Pr-doped Nd-123. The solid curve is a fit to Eq. (1).

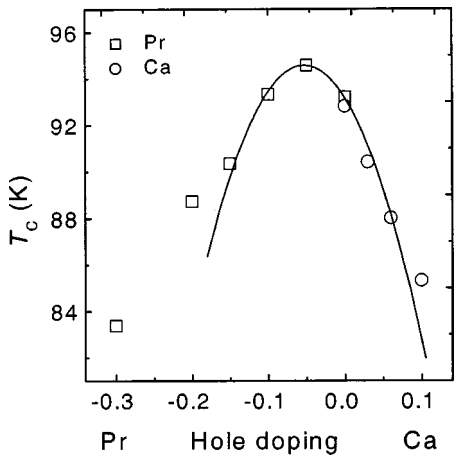

FIG. 5. Superconducting transition temperatures for Pr- and Ca-doped samples vs hole doping. For Pr, negative x indicates electron doping. For the Pr-doped samples, the observed T_c has been corrected for the linear term of Eq. (1) by subtracting Bx ($x<0, B=205$ K). The solid curve is a fit of Eq. (1) with $y=0$ and $B=0$. Data for Ca doping in Nd-123 samples have been taken from Ref. 36.

IV. RESULTS AND ANALYSES

A. Resistivity measurements

The temperature dependencies of the resistivity, ρ, for the $Nd_{1-x}Pr_xBa_2Cu_3O_{7-\delta}$ samples are shown in Fig. 3. The scale for ρ was obtained by taking into account the porosity of sintered samples with an estimated correction of the mass density of 12%.[34] Pr doping results in a larger normal state resistivity, a lower T_c and a change from a metal-like to a semiconductorlike behavior at low temperatures and high doping concentration. As shown in Fig. 4, the room temperature resistivity, $\rho_{290\,\mathrm{K}}$, of these samples increases almost linearly with increasing doping level for $x \leqslant 0.15$ and increases faster for larger x. The results suggest a simple impurity effect for $x \leqslant 0.15$, where $d\rho/dT$ is constant at room temperature, and a weakening metallic state at larger x where $(d\rho/dT)_{290\,\mathrm{K}}$ decreases. These observations are in agreement with a schematic picture[35] for the variation of the density of states around the Fermi energy with doping concentration. With increasing Pr content the Fermi energy moves towards the localized part of the band at the tail of the density of states, and with further doping it enters the localized part and causes the conductivity to strongly decrease. This change is consistent with a decreasing hole concentration in the planes, which is described later. The linear change in $\rho_{290\,\mathrm{K}}$ at low doping level is also in agreement with observations on Ca^{2+}-doped Nd-123,[36] as illustrated in Fig. 4 by the similar behavior on the hole-doped side.

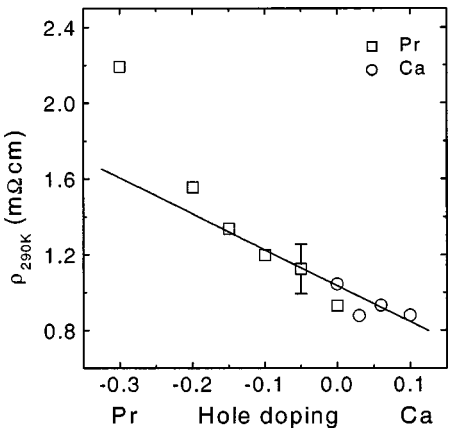

FIG. 4. The room temperature resistivity $\rho_{290\,\mathrm{K}}$, vs hole doping x. Pr reduces ($x<0$) and Ca increases ($x>0$) the number of holes. Data for Ca doping in Nd-123 samples have been taken from Ref. 36. The solid line is a guide to the eye. The error bar illustrates the uncertainty, which is almost entirely due to errors in the geometrical form factors of the samples.

T_c defined from the midpoint of the resistive transition is shown in the inset of Fig. 3. Equation (1) with $y=0$ was fitted to these data, which gave $B=205$ K in good agreement with B in related work.[12,35] When the linear term $-Bx = -205x$ was subtracted from the observed T_c of the Pr-doped samples, the resulting concentration dependence of T_c is paraboliclike up to $x \leqslant 0.15$ as illustrated by the open squares in Fig. 5. This parabola has the form $T_c(K) = 94.58 - 612(0.048 - 0.91x)^2$ (K), confirming a Pr valence close to $+4$ (3.91) at low Pr concentrations. At larger Pr concentrations there are deviations towards a slower T_c dependence on doping concentration supporting a limit for pure Pr^{4+} doping in Nd-123 of about $x \approx 0.15$. The position of the maximum of the parabola in Fig. 5 suggests that our pure Nd-123 has an overdoping of holes of 4.8% per 123 unit cell.

B. Neutron diffraction

The Rietveld refinements of the neutron diffraction patterns of the $Nd_{1-x}Pr_xBa_2Cu_3O_{7-\delta}$ system including structural parameters, atomic positions, z, along the c axis, occupation numbers, n, isotropic temperature factors, β_{iso}, anisotropic temperature factors, β_{ii}, for the chain O1 position, and oxygen content, δ, are listed in Table I. The R

TABLE I. Structural parameters for $Nd_{1-x}Pr_xBa_2Cu_3O_{7-\delta}$. The relative position along the *c*-axis, *z*, the occupation number *n*, the isotropic temperature factor, β_{iso}, and the oxygen deficiency, δ, are given. For O1, anisotropic temperature factors were used on the form $\exp[-(\beta_{11}h^2+\beta_{22}k^2+\beta_{33}l^2)]$. The Nd(Pr) site occupancies were refined with the constraint that the Nd site is fully occupied. The numbers in the parentheses are the estimated standard deviation in the last digit.

x (%)		0	5	10	15	20	30
a (Å)		3.8628(2)	3.8617(2)	3.8602(2)	3.8584(2)	3.8602(2)	3.8579(2)
b (Å)		3.9134(2)	3.9145(2)	3.9160(2)	3.9156(2)	3.9188(2)	3.9183(2)
c (Å)		11.7525(7)	11.7453(8)	11.7434(8)	11.7342(7)	11.7368(7)	11.7324(7)
V (Å)		177.66(2)	177.55(2)	177.52(2)	177.28(2)	177.55(2)	177.35(2)
Nd	β_{iso}(Å^2)	0.23(5)	0.31(6)	0.22(6)	0.26(7)	0.36(6)	0.30(7)
	n	1	0.951(4)	0.902(4)	0.851(4)	0.802(4)	0.701(4)
Pr	*n*	0	0.049(6)	0.098(6)	0.149(6)	0.198(6)	0.299(6)
Ba	*z*	0.1815(3)	0.1817(3)	0.1813(3)	0.1811(3)	0.1811(3)	0.1809(3)
	β_{iso}(Å^2)	0.37(6)	0.43(7)	0.34(6)	0.41(6)	0.40(6)	0.43(6)
Cu(1)	β_{iso}(Å^2)	0.75(6)	0.83(7)	0.69(7)	0.73(7)	0.72(7)	0.75(7)
Cu(2)	*z*	0.3493(2)	0.3495(2)	0.3493(2)	0.3493(2)	0.3497(2)	0.3494(2)
	β_{iso}(Å^2)	0.43(4)	0.40(4)	0.44(4)	0.40(4)	0.44(4)	0.48(4)
O(2)	*z*	0.3709(3)	0.3716(4)	0.3719(3)	0.3716(3)	0.3725(3)	0.3728(3)
	β_{iso}(Å^2)	0.63(7)	0.81(8)	0.69(8)	0.72(8)	0.79(8)	0.78(8)
O(3)	*z*	0.3716(4)	0.3717(4)	0.3721(4)	0.3723(4)	0.3726(4)	0.3726(4)
	β_{iso}(Å^2)	0.66(7)	0.69(7)	0.70(7)	0.70(7)	0.77(7)	0.76(7)
O(4)	*z*	0.1579(3)	0.1578(3)	0.1580(3)	0.1580(3)	0.1580(3)	0.1583(3)
	β_{iso}(Å^2)	0.82(7)	0.69(8)	0.70(8)	0.67(7)	0.66(7)	0.66(7)
O(1)	β_{11}	0.048(5)	0.059(6)	0.046(6)	0.047(6)	0.056(6)	0.050(6)
	β_{22}	0.006(4)	0.017(5)	0.007(4)	0.008(4)	0.009(4)	0.008(4)
	β_{33}	0.0023(5)	0.0021(6)	0.0022(6)	0.0025(6)	0.0026(6)	0.0019(6)
	n	0.950(5)	0.968(7)	0.952(6)	0.974(6)	0.967(6)	0.960(6)
O(5)	*n*	0.056(5)	0.067(6)	0.048(6)	0.046(5)	0.064(6)	0.062(5)
δ		−0.006	−0.035	−0.000	−0.020	−0.031	−0.022
χ		2.35	2.31	2.16	2.17	2.19	2.14
R_p (%)		7.93	9.13	8.87	8.50	8.52	9.20
R_{wp} (%)		8.86	9.61	9.34	9.30	9.41	9.46
R_{expt} (%)		5.77	6.32	6.35	6.30	6.35	6.47
R_{Bragg} (%)		2.24	2.68	2.65	2.62	2.50	2.79

values and χ factor, giving different measures of the quality of fits, are small and indicate a good quality of the analyses.

The results for Pr and Nd occupation on Nd sites showed that the Pr/Nd ratio was close to nominal values for *all* samples. This is not expected if some Nd and/or some Pr would have entered the Ba site. This result in Table I is strong support that our samples have the stoichiometry of the $Nd_{1-x}Pr_xBa_2Cu_3O_{7-\delta}$ formula. Since it has been suggested that Pr substitution on Ba site causes the destruction of superconductivity,[37] we further investigated this issue by refinements including the Ba-site occupancy.[27] Within two standard deviations in the result for n_{Pr}(Ba), there was no indication from our refinements that Pr occupies the Ba sites. For the $x=0$ sample, replacing n_{Pr}(Ba) by n_{Nd}(Ba) and allowing n_{Nd}(Nd) to vary freely, the results similarly showed no evidence of Nd on the Ba site. It can furthermore be noted that from studies of $Nd_{1.05}Ba_{1.95-x}Pr_xCu_3O_{7-\delta}$ it was inferred that Pr behaves similarly to other rare earths on the Ba site.[23] The contention of a depression of T_c due to Pr on the Ba site therefore does not seem well supported.

We briefly summarize our findings indicating the expected sample stoichiometry. No impurity phases have been detected in our sensitive x-ray experiments, or in the EDS analyses, indicating the correct overall composition for the 123 samples. No evidence is found from the Rietveld refinements of Pr entering the Ba site or, for the $x=0$ sample, for Nd on the Ba site. This is further supported by the refinements on the Nd site, which showed a Pr/Nd ratio close to the nominal one for all samples. Finally, the EDS analyses indicated that the Ba/Cu ratios in the 123 phases of two samples was constant over the investigated sample area, in agreement with the other structural investigations.

As seen in Table I all lattice parameters vary slightly with doping with the largest change of the *c*-axis lattice parameter. This is in contrast to Pr-doped Y-123,[22] where the largest changes are in the *a*- and *b*-axis parameters. The orthorhombic distortion, defined as $(b-a)/(b+a)$, increases with doping in Nd(Pr)-123 in contrast to $Y_{1-x}Pr_xBa_2Cu_3O_{7-\delta}$.[22] As can be seen in Table I, the *b*-axis lattice parameter increases and the *a*-axis parameter slightly decreases up to $x=0.15$ and

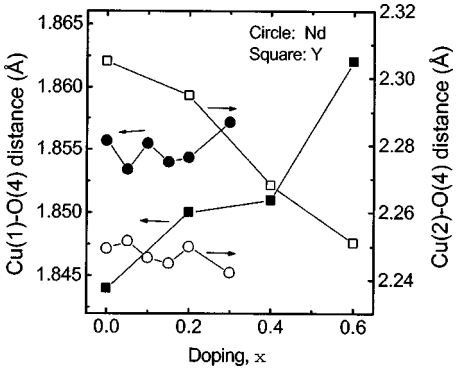

FIG. 6. Cu1-O4 distance for $Nd_{1-x}Pr_xBa_2Cu_3O_{7-\delta}$ (●) and $Y_{1-x}Pr_xBa_2Cu_3O_{7-\delta}$, (■) (left scale). Cu2-O4 distance for $Nd_{1-x}Pr_xBa_2Cu_3O_{7-\delta}$, (○) and $Y_{1-x}Pr_xBa_2Cu_3O_{7-\delta}$, (□) (right scale). Data for Y based samples have been taken from Ref. 22.

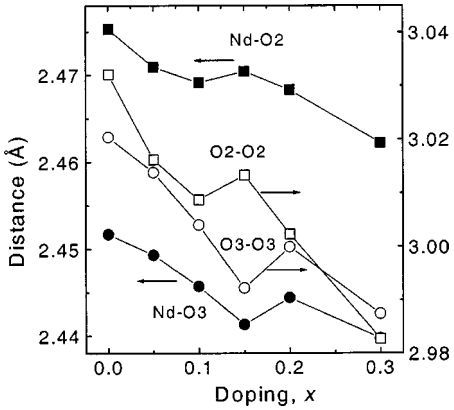

FIG. 7. Nd(Pr)-O2, Nd(Pr)-O3, O2-O2, and O3-O3 distances vs Pr doping content x for $Nd_{1-x}Pr_xBa_2Cu_3O_{7-\delta}$.

is constant at higher x. On the other hand, in Y(Pr)-123 the a-axis lattice parameter increased faster than the b-axis-parameter.[22]

The Cu1-O4 and Cu2-O4 distances have been considered to be important for the charge transfer between chains and planes. Figure 6 shows a comparison of these distances for Pr-doped Nd-123 with published results for Y(Pr)-123.[22] When Pr replaces Nd in Nd-123, the apical oxygen atom O4 remains stationary (Table I) and the Cu2-O4 distance decreases slightly while the Cu1-O4 distance is almost constant. As can be seen in Fig. 6, these distances change more strongly and in the opposite direction in $Y_{1-x}Pr_xBa_2Cu_3O_{7-\delta}$, which suggests a different carrier distribution between planes and chains. Smaller variations in atomic distances in Nd(Pr)-123 are generally found when comparing with corresponding calculations for Y(Pr) 123 from data in Ref. 22.

Small changes in the doping dependence of structural parameters which are suggestive of a Pr^{4+} valence at low concentrations can be discerned also in Nd(Pr)-123. Figure 7 shows the distances Nd(Pr)-O2, Nd(Pr)-O3, O2-O2, and O3-O3 vs the Pr doping concentration x. All these distances decrease with increasing x, as expected from the much smaller ionic radius for Pr^{4+} than for Nd^{3+}, but not expected for Pr^{3+} which has an ionic radius slightly larger than Nd^{3+}.[38] Similarly, there is a contraction of the c-axis lattice parameter with doping at small x in Table I, reflecting the smaller Pr^{4+}, which flattens out at $x \geqslant 0.15$, consistent with a change of valence towards Pr^{3+}.

The large differences between the results for Pr doping in Y- and Nd-123 are noteworthy. In Ref. 22 the measurements on doped samples were limited to $x \geqslant 0.2$, and Pr is therefore likely 3 valent. In part these differences can therefore be understood from ionic size factors. The ionic radius of Pr^{3+} is only 2% larger than for Nd^{3+}, but 11% larger than for Y^{3+},[38] and a stronger doping dependence of structural parameters in Y-123 can be expected. However, other differences noticed above, such as the different doping dependence of the orthorhombic distortion, are not readily understood in this picture.

It has been shown that superconductivity in R-123 compounds is lost when the buckling angle of the CuO_2 plane becomes smaller than a critical value of about 6.35°.[39] Here the buckling angles φ_2 and φ_3 are defined as in Fig. 1. Chmaissem *et al.*[40] observed a clear scaling between T_c and buckling angle, φ_2, with both quantities displaying a maximum at the same oxygen content, $7-\delta$, for different doping levels x, while T_c increased and φ_2 decreased for increasing x. They concluded that the observation of a maximum in the buckling at the maximum of T_c vs $7-\delta$, indicates that a structural response competes with superconductivity when the composition was changed to increase T_c. We found that the buckling angle of the CuO_2 planes for $Nd_{1-x}Pr_xBa_2Cu_3O_{7-\delta}$ increases with increasing Pr concentration up to $x \approx 0.15$. At larger x-values deviations are observed (Fig. 8). We also note that the highest T_c occurs for the pure sample with the smallest buckling angle, which is in agreement with previous results.[40–42]

Some results of the neutron diffraction experiments are briefly summarized. Structural distortions with Pr substitution in $Nd_{1-x}Pr_xBa_2Cu_3O_{7-\delta}$ are small. The position of the apical oxygen atom does not depend on the Pr doping concentration. The atomic distances between Nd(Pr) and oxygen atoms decrease with increasing Pr doping concentration, and the buckling angles of the planes increase up to $x \approx 0.15$. The occupation of O1, n_{O1}, and O5, n_{O5} are constant within 0.01. Overall, the oxygen content was roughly constant.

C. Bond valence sums

Bond valence sums were calculated with the constant valence and mixed valence methods described in Sec. III. With the CV method we considered a Pr valence +4 at $x \leqslant 0.15$ and +3 for $x > 0.15$ using different lengths L_o for these two valences in Eq. (2). In the mixed valence method different valences for Cu (+1, +2, and +3) and Pr (+3 and +4) were used for the calculation of the oxygen BVS. The results for both BVS calculations are shown in Table II. Error estimations are shown in several cases. Similar estimates were obtained for the other compositions. Some trends for increasing Pr doping are the constant and near constant Cu2 and Cu1 valences, the small decrease of V_+, and the decrease of plane and chain charge concentrations.

In both calculation methods, the total hole concentration in the planes, $V_{\text{-pl}}$ and chains, $V_{\text{-ch}}$, have similar doping

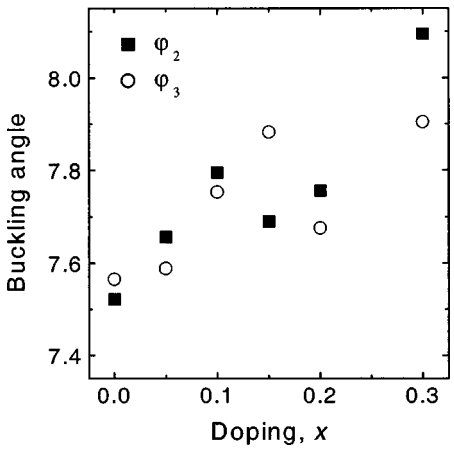

FIG. 8. The buckling angles in the Cu-O plane vs doping x. φ_2 and φ_3 are defined in Fig. 1.

dependencies, decreasing with an increasing Pr concentration. However, the actual values for the MV method are smaller than for the CV method. We also recalculated $V_{\text{-pl}}$ with the MV method for $YBa_2Cu_3O_{7-\delta}$ with $0.05 \leqslant \delta \leqslant 0.65$ using data from Ref. 32. It was again found that the trends in BVSs were stable, while the actual values were smaller for the MV calculations than for the CV results.

Another method to estimate the hole concentration in the planes is the universal relation between the room temperature thermoelectric power, $S_{290\,\text{K}}$ and $V_{\text{-pl}}$, which was found by Obertelli *et al.*[43] For comparison, results for $V_{\text{-pl}}$ estimated from measurements of $S_{290\,\text{K}}$ for the same samples,[44] have been included in Table II. It can be seen that these results agree qualitatively with the BVS calculations with a similar trend of $V_{\text{-pl}}$ vs x. The actual values are more uncertain. For the pure sample, the estimate of $V_{\text{-pl}}$ from $S_{290\,\text{K}}$ was 33% and 60% larger than obtained from CV and MV methods, respectively.

As can be seen in Table II, the Cu2 valence is constant. A possible small increase in the BVSs for O2, and O3 for increasing x, and the tendency for a weak decrease of V_+, support that there is no hole localization on oxygen either. BVSs for O4 and Ba are, within error bars, roughly constant. The Cu1-O4 distance is almost constant (Fig. 6). There is thus no evidence of charge transfer between a chain and plane. These results suggest that a likely reason for the decrease of $V_{\text{-pl}}$ is the localization of holes on Nd(Pr) sites. In this process the valence on the Nd(Pr) site will increase somewhat, in agreement with the results in Table II. This should be distinguished from the model of the CV calculations, where a decrease of the Pr valence from +4 to +3 is imposed at $x=0.15$ to describe the valence change. This valence change has, overall, a rather small effect on $V_{\text{-pl}}$, as seen by the limited differences between BVS results in the CV and MV calculations, and by the fairly smooth results of $V_{\text{-pl}}$ as a function of x, with no apparent discontinuity at $x=0.15$.

TABLE II. Bond valence sums (BVS) for the different atoms in $Nd_{1-x}Pr_xBa_2Cu_3O_{7-\delta}$ with the constant valence method. $V_{\text{-pl}}$ $V_{\text{-ch}}$ and V_+ give the average hole density in the plane, chains, and preference for distribution of holes on oxygen sites, respectively. The numbers in the parentheses are the estimated errors in the last digit(s). For comparison several BVS results calculated with the mixed valence (MV) method are also given. $V_{\text{-pl}}(S)$ denotes an estimate obtained from the room temperature thermoelectric power.

x (%)	0	5	10	15	20	30
Nd	3.037(9)	3.065	3.088	3.095	3.120	3.137
Ba	2.152(11)	2.163	2.143	2.162	2.150	2.145
Cu1	2.292(6)	2.356	2.283	2.331	2.345	2.295
Cu2	2.117(2)	2.114	2.112	2.118	2.102	2.110
O1	1.750(1)	1.748	1.756	1.764	1.758	1.768
O1 (MV)	1.791(1)	1.798	1.795	1.810	1.806	1.811
O2	2.018(12)	2.032	2.035	2.043	2.039	2.049
O2 (MV)	2.035(13)	2.047	2.049	2.057	2.057	2.070
O3	2.013(14)	2.025	2.028	2.039	2.033	2.042
O3 (MV)	2.029(14)	2.039	2.041	2.051	2.050	2.062
O4	1.932(5)	1.934	1.936	1.942	1.933	1.938
O4 (MV)	1.963(6)	1.970	1.965	1.976	1.968	1.968
O5	1.781(1)	1.780	1.789	1.798	1.793	1.801
O5 (MV)	1.825(1)	1.834	1.831	1.847	1.842	1.845
$V_{\text{-pl}}$	0.087(18)	0.057(20)	0.049(19)	0.037(19)	0.030(19)	0.019(20)
$V_{\text{-pl}}$ (MV)	0.054(18)	0.028	0.022	0.010	−0.005	−0.022
$V_{\text{-pl}}(S)$	0.131	0.121	0.116	0.109	0.103	0.093
$V_{\text{-ch}}$	0.524(6)	0.528	0.517	0.508	0.503	0.488
$V_{\text{-ch}}$ (MV)	0.483(6)	0.476	0.477	0.460	0.453	0.446
V_+	−0.148(18)	−0.170	−0.175	−0.200	−0.174	−0.201
V_+ (MV)	−0.180(18)	−0.199	−0.201	−0.226	−0.209	−0.242
T_c (K)	92.2	84.3	72.8	59.7	57.7	21.9

From Table II it is further found that V_{O1} and V_{O5} increase slightly with increasing Pr doping, while V_{Cu1} fluctuates. In terms of Eq. (4), the decreasing $V_{\text{-ch}}$ is thus dominated by the increasing O1 and O5 BVSs. The fluctuations of V_{Cu1} can be seen to correlate with the fluctuations in oxygen chain occupancy, n_{O1}, from Table I. This is expected from the bonding relations and illustrates the sensitivity of the BVS calculations.

It is interesting to compare these results for $V_{\text{-pl}}$ with Pr-doped Y-123. Neutron diffraction results for $Y_{1-x}Pr_xBa_2Cu_3O_{7-\delta}$ at $x=0$, 0.2, 0.4, 0.6, and 1, have been published,[22] and we have made BVS calculations from these data.[22] Figure 9 shows T_c vs $V_{\text{-pl}}$ for Pr-doped Y- and Nd-123. The results from the MV calculations show a similar trend as those from the CV method but are somewhat smaller. For both calculation methods and both alloy systems the results are qualitatively similar with a strong decrease of T_c for decreasing $V_{\text{-pl}}$. For CV calculations, the preferred method, T_c for both Y- and Nd-based-123 falls to zero for $V_{\text{-pl}}$ in the interval 0.02–0.05, in fair agreement with the lower limit $p_{\min}$ of the range of hole concentrations in the planes, p, where superconductivity is observed,[9] as briefly described in Sec. I.

As mentioned, bond lengths changes often have opposite signs in Nd(Pr)-123 compared to Y(Pr)-123 and are significantly smaller in magnitude for the Nd-based alloys. Hence it is difficult to identify any particular bond length of special importance for the change of T_c with Pr doping in these two alloy systems. BVS calculations, on the other hand, sense changes in weighed sums of bond lengths in an alloy series. Our results show that BVS calculations can identify $V_{\text{-pl}}$ as such a crucial parameter in alloy systems with markedly different doping effects on bond lengths.

The preference for holes to go to the oxygen ions in the CuO_2 plane, V_+, was linearly correlated by Tallon[20] to the maximum attainable T_c in a particular system. From the BVS results (Table II), V_+ decreases with decreasing T_c. The trends for both types of BVS calculations are similar to that expected for optimally doped ceramic samples.[20] However, the slope dT_c/dV_+ is much larger (about twenty times) for Pr-doped Nd-123 than for several systems studied in Ref. 20. In contrast the data for $Y_{1-x}Pr_xBa_2Cu_3O_{7-\delta}$[22] indicate that V_+ remains essentially constant.

V. DISCUSSION AND CONCLUSIONS

The problem of the depression of T_c in $Nd_{1-x}Pr_xBa_2Cu_3O_{7-\delta}$ has been studied by neutron diffraction and BVS calculations on sintered samples. In this intensively debated field of study, concerns have been raised also about sample stoichiometry in Pr-doped samples, and about the reliability of semiempirical results from BVS calculations. Particular attention has therefore been paid to these points. Structural investigations and characterization were made by x-ray diffraction, EDS analyses in a scanning electron microscope, resistivity measurements, and Rietveld refinements of site occupancies. The results showed phase pure samples of the expected stoichiometry. In particular, no evidence was found of Ba on Nd sites, nor of Pr on Ba site. The

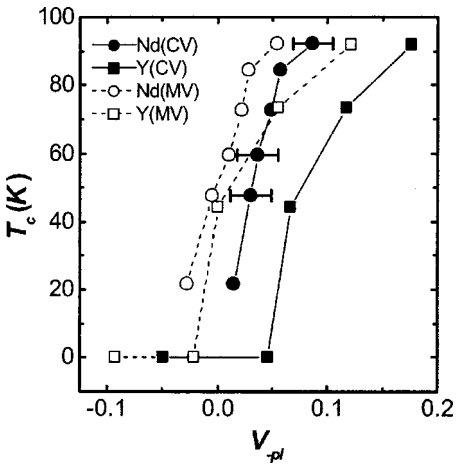

FIG. 9. T_c vs $V_{\text{-pl}}$ for Pr-doped Y-123 (circles) and Nd-123 (squares) for both BVS calculations. Typical error estimates of the BVS calculations are shown by a bar for some data points. Corresponding data for Y-based samples have been calculated from data from Ref. 22.

trends of the BVS results were checked by using two models, the CV and MV methods, and in addition by comparing with calculations made from published structural results[22] for $Y_{1-x}Pr_xBa_2Cu_3O_{7-\delta}$.

It was found that charge depletion in the CuO_2 plane is an important mechanism, and the structural results further suggest that this occurs by hole localization on the Nd(Pr) site. The qualitative similarity between all four calculations supports the consistency of our BVS analyses.

In the literature on Pr-doped superconductors, propositions of depletion of mobile charge in the CuO_2 plane, and localization, have been made before. Three recent examples are the following: Thampi *et al.*[45] concluded from studies of electrical transport and magnetic properties that T_c is depressed in Pr-doped Eu-123 due to the hole localization. From analyses of resistivity results Tomkowicz[19] suggested a hole trapping mechanism all the way to the critical concentration of $x \approx 0.6$ in $Ho_{1-x}Pr_xBa_2Cu_3O_{7-\delta}$. From analyses of the thermoelectric power in terms of different semiempirical models, we suggested[46] that charge localization is an important contribution to the T_c depression in charge neutrally doped $Nd(Ca_xPr_x)$-123.

In the present paper we have used a generalized approach, taking into account both hole filling and hole localization. Hole filling takes place at low concentrations, and is arrested at the apparent valence shift of Pr^{4+}. This is modeled in our BVS calculations in the CV method by taking the Pr valence to be 4^+ up to $x=0.15$ and 3^+ for larger x. The range for hole localization is found from the calculations. The results show a progressive depletion of planar charge for increasing Pr concentration for both Nd(Pr)- and for Y(Pr)-123, over the range from $x=0$ up to close to the critical Pr concentration x_c, where T_c disappears. x_c is about twice as large in Y(Pr)- as in Nd(Pr)-123. Yet our results for $V_{\text{-pl}}$ at x_c in the CV method (0.02–0.05) agree qualitatively for both alloy systems, and are also in agreement with previous results for p in other alloy systems.[20,47]

The similarity between these results and those calculated for $V_{\text{-pl}}$ from the MV method place further emphasis on the importance of charge depletion in the planes, and shows that this result is also found without an initial assumption about the Pr valence at small dopings. However, for the MV method the agreement with other estimates of p is lost, thus supporting the preference of the CV calculations. In fact, the agreement between previous results and our CV results for $V_{\text{-pl}}(x=x_c)$ in two alloy systems with widely different doping dependencies of the bond lengths as well as with large differencies in x_c, suggests the picture that charge depletion in the planes is a general mechanism for depression of T_c in Pr-doped (R)-123.

ACKNOWLEDGMENTS

We thank I. Bryntse and M. Valldor, Stockholm University, for help with sample preparation and x-ray analysis, and H. Rundlöf, Studsvik, for skilled assistance with the neutron diffraction experiments and for useful discussions. We are grateful to G. Svensson, Stockholm University, for performing the EDS analyses and to him and P. E. Werner, Stockholm University, for several clarifying discussions on the Rietveld refinement procedures. Financial support from the Swedish Research Agency Vetenskapsrådet (VR) and the Swedish OXIDE Program, and from the Iranian Ministry of Science, Research, and Technology (MSRT) are gratefully acknowledged.

[1] Y. Xu and W. Guan, Phys. Rev. B **45**, 3176 (1992).
[2] Y. Dalichaouch, M. S. Torikachvili, E. A. Early, B. W. Lee, C. L. Seaman, K. N. Yang, H. Zhou, and M. B. Maple, Solid State Commun. **65**, 1001 (1988).
[3] J. J. Neumeier, T. Bjørnholm, M. B. Maple, and I. K. Schuller, Phys. Rev. Lett. **63**, 2516 (1989).
[4] A. Kebede, C. S. Jee, J. Schwegler, J. E. Crow, T. Mihalisin, G. H. Myer, R. E. Salomon, P. Schlottmann, M. V. Kuric, S. H. Bloom, and R. P. Guertin, Phys. Rev. B **40**, 4453 (1989).
[5] G. Y. Guo and W. M. Temmerman, Phys. Rev. B **41**, 6372 (1990); R. Fehrenbacher and T. M. Rice, Phys. Rev. Lett. **70**, 3471 (1993); A. I. Liechtenstein and I. I. Mazin, *ibid.* **74**, 1000 (1995).
[6] H. B. Blackstead, J. D. Dow, D. B. Chrisey, J. S. Horwitz, M. A. Black, P. J. McGinn, A. E. Klunzinger, and D. B. Pulling, Phys. Rev. B **54**, 6122 (1996).
[7] Z. Zou, J. Ye, K. Oka, and Y. Nishihara, Phys. Rev. Lett. **80**, 1074 (1998).
[8] V. N. Narozhny and S. L. Drechsler, Phys. Rev. Lett. **82**, 461 (1999); Z. Zou and Y. Nishihara, *ibid.* **82**, 462 (1999).
[9] M. R. Presland, J. L. Tallon, R. G. Buckly, R. S. Liu, and N. E. Flower, Physica C **176**, 95 (1991).
[10] G. Cao, J. Bolivar, J. W. O'Reilly, J. E. Crow, R. J. Kennedy, and P. Pernambuco-Wise, Physica B **186-188**, 1004 (1993).
[11] M. Andersson, Ö. Rapp, T. L. Wen, Z. Hegedüs, and M. Nygren, Phys. Rev. B **48**, 7590 (1993).
[12] P. Lundqvist, C. Tengroth, Ö. Rapp, R. Tellgren, and Z. Hegedüs, Physica C **269**, 231 (1996).
[13] P. Lundqvist, P. Grahn, Ö. Rapp, and I. Bryntse, Physica C **289**, 137 (1997).
[14] P. Lundqvist, Ö. Rapp, R. Tellgren, and I. Bryntse, Phys. Rev. B **56**, 2824 (1997).
[15] F. W. Lytle, G. van der Laan, R. B. Greegor, E. M. Larsson, C. E. Violet, and J. Wong, Phys. Rev. B **41**, 8955 (1990).
[16] M. Andersson, Ö. Rapp, and R. Tellgren, Physica C **205**, 105 (1993).
[17] H. Iwasaki, J.-I. Sugawara, and N. Kobayashi, Physica C **185-189**, 1249 (1991).
[18] A. Okada, J. Arai, and K. Umezawa, Physica C **235-240**, 817 (1994).
[19] Z. Tomkowicz, Physica C **320**, 173 (1999).
[20] J. L. Tallon, Physica C **168**, 85 (1990).
[21] J. L. Tallon, C. Bernard, H. Shaked, R. L. Hitterman, and J. D. Jorgensen, Phys. Rev. B **51**, R12 911 (1995).
[22] J. J. Neumeier, T. Bjørnholm, M. B. Maple, J. J. Rhyne, and J. A. Gotaas, Physica C **166**, 191 (1990).
[23] M. J. Kramer, K. W. Dennis, D. Falzgraf, R. W. McCallum, S. K. Malik, and W. B. Yelon, Phys. Rev. B **56**, 5512 (1997).
[24] K. E. Johansson and P. E. Werner, J. Phys. E **13**, 1289 (1989).
[25] Some further details about the Studsvik neutron spectrometer; Collimators were placed before the monochromator, after the monochromator, and before the detector. The resolutions were about, 50, 30, and 10 arcmin, respectively. The resolution in 2θ above about 30° varies between 0.6% and 0.9% with the minimum value at about 60°.
[26] H. M. Rietveld, J. Appl. Crystallogr. **2**, 65 (1969).
[27] We assumed fully occupied Nd and Ba sites and nominal Pr stoichiometry. The following five equations were used. $b(A)$ denotes the scattering length of element A. (i) $n_{\text{Nd}}(\text{Nd})+n_{\text{Pr}}(\text{Nd})=1$. (ii) $n_{\text{Nd}}(\text{Nd})b(\text{Nd})+n_{\text{Pr}}(\text{Nd})b(\text{Pr})$ is the measured scattering density from Nd site. (iii) $n_{\text{Ba}}(\text{Ba})+n_{\text{Pr}}(\text{Ba})=1$ for each Ba site. (iv) $n_{\text{Ba}}(\text{Ba})b(\text{Ba})+n_{\text{Pr}}(\text{Ba})b(\text{Pr})=$measured scattering density from Ba site. (v) $n_{\text{Pr}}(\text{Nd})+2n_{\text{Pr}}(\text{Ba})=x$.
[28] Small features in both panels of Fig. 2 at $2\theta\approx 15°$ and between 40 and 45° are experimental artifacts. They were similar in the neutron diffraction experiments and absent in x-ray diffraction.
[29] I. D. Brown and R. D. Shannon, Acta Crystallogr., Sect. A: Cryst. Phys., Diffr., Theor. Gen. Crystallogr. **29**, 266 (1973).
[30] I. D. Brown, J. Solid State Chem. **82**, 122 (1989).
[31] I. D. Brown and D. Altermatt, Acta Crystallogr., Sect. B: Struct. Sci. **41**, 244 (1985).
[32] R. J. Cava, A. W. Hewat, E. A. Hewat, B. Batlogg, M. Marezio, K. M. Rabe, J. J. Krajeweski, W. F. Peck, and L. W. Rupp, Physica C **165**, 419 (1990).
[33] P. Lundqvist, Czech. J. Phys. **46-S2**, 947 (1996).
[34] P. Lundqvist, Ph.D. thesis, Royal Institute of Technology, Stockholm, Sweden, 1998, TRITA-FYS 5241.
[35] S. R. Ghorbani, P. Lundqvist, M. Andersson, M. Valldor, and Ö. Rapp, Physica C **353**, 77 (2001).
[36] S. R. Ghorbani, M. Andersson, P. Lundqvist, M. Valldor, and Ö. Rapp, Physica C **339**, 245 (2000).
[37] H. B. Blackstead and J. D. Dow, Phys. Rev. B **51**, 11 830 (1995).

[38] R. D. Shannon, Acta Crystallogr., Sect. A: Cryst. Phys., Diffr., Theor. Gen. Crystallogr. **32**, 751 (1976).
[39] M. Guillaume, P. Allenspach, W. Henggeler, J. Mesot, B. Roessli, U. Staub, P. Fischer, A. Furrer, and V. Trounov, J. Phys.: Condens. Matter **6**, 7963 (1994).
[40] O. Chmaissem, J. D. Jorgensen, S. Short, A. Knizhnik, Y. Eckstein, and H. Shaked, Nature (London) **397**, 45 (1999).
[41] B. Büchner, M. Breuer, A. Freimuth, and A. P. Kampf, Phys. Rev. Lett. **73**, 1841 (1994).
[42] E. Kaldis, J. Röhler, E. Liarokapis, N. Poulakis, K. Conder, and P. W. Loeffen, Phys. Rev. Lett. **79**, 4894 (1997).
[43] S. D. Obertelli, J. R. Cooper, and J. L. Tallon, Phys. Rev. B **46**, 14 928 (1992).
[44] S. R. Ghorbani and Ö. Rapp, Physica C **388-389**, 351 (2003).
[45] R. S. Thampi, S. Rayaprol, K. Mavani, D. G. Kuberkar, M. R. Gonal, R. Prasad, and G. Kulkarni, Physica C **355**, 23 (2001).
[46] S. R. Ghorbani, M. Andersson, and Ö. Rapp, Phys. Rev. B **66**, 104519 (2002).
[47] J. L. Tallon and N. E. Flower, Physica C **204**, 237 (1993).